SOME OBSERVATIONS OF THE VIBRATIONS OF SLENDER ROTATING SHAFTS

John Dugundji
Monica M. Buellesbach
Mary A. Wright

GT&PDL Report No. 163 March 1982

GAS TURBINE & PLASMA DYNAMICS LABORATORY
MASSACHUSETTS INSTITUTE OF TECHNOLOGY
CAMBRIDGE, MASSACHUSETTS

SOME OBSERVATIONS OF THE VIBRATIONS OF SLENDER ROTATING SHAFTS

John Dugundji
Monica M. Buellesbach
Mary A. Wright

GT&PDL Report No. 163 March 1982

Abstract

The linear theory of a slender, initially bowed, rotating shaft is reviewed for both free and forced vibrations, and found to compare well with a simple experiment on such a shaft. The shaft behavior passing through the critical speed is described in detail, and the maximum bowed-out static deflection of the shaft was found dependent on the external damping and the initial bowing. The amplitude of the oscillatory deflections of the shaft due to gravity loads increased somewhat near the critical speed, but these increases were small compared to the large static deflection of the shaft. During rapid passage through the critical speed, low frequency whirling modes were excited transiently. At higher rotation speeds, the second critical speed was observed, and also the first mode was excited subharmonically and appeared as a backward whirl mode relative to the rotating shaft.

Acknowledgements

The authors wish to acknowledge the assistance of Allan Shaw and Donald Weiner in setting up the experiment. Also, they wish to acknowledge some preliminary work on this experiment by Stephen Levin.

Table of Contents

Nomenclature

A_{OB}	observed amplitude
A_s, B_c	amplitudes
c_s, c_A	structural and aerodynamic damping
F_{BY}, F_{BZ}	forces on bearings
g	acceleration of gravity
h_η, h_ζ	initial bowing of shaft
h	initial bow = $\sqrt{h_\eta^2 + h_\zeta^2}$
i	$\sqrt{-1}$
k_η, k_ζ	shaft stiffnesses
ℓ	length of shaft
M	total mass of shaft
m	mass per unit length
p	characteristic root = $a + i\omega$
q_η, q_ζ	elastic deflection of shaft
$q_{\eta o}$, $q_{\zeta o}$	static elastic deflection of shaft
t	time
y_c, z_c	absolute displacement of C.G.
ζ_S, ζ_A	structural and aerodynamic damping ratios
ψ	angle of rotation
Ω	rotation speed
ω_η, ω_ζ	natural frequencies of shaft
ω_N	natural frequency, $\omega_N = \omega_\eta = \omega_\zeta$
ω_1, ω_2	frequencies relative to shaft

1. Introduction

The vibrations of a rotating shaft have always been an important and interesting phenomenon in mechanical systems. The occurrence of unbalance vibrations, critical speeds, and associated whirling phenomena is well known and has been described by many authors. Den Hartog [1] gives a good description of the physical and practical problems involved with these rotating shafts, Bolotin [2] and Ziegler [3] give good discussions of theoretical aspects of the problem. Vance and Royal [4] give a good discussion of the applications to turbine engines. Gunter [5] gives a good extensive discussion of theoretical and practical design considerations involving details of support motions, damping, nonlinear effects, hydrodynamic bearings, etc. Still, in many cases, the consequences of passing through a critical speed region and the amplitude of the resulting vibrations is often difficult to assess.

The present article reviews the linear theory for free and forced vibrations of a slender, initially bowed, rotating shaft and compares it with a simple experiment on such a shaft. It attempts thereby to give a clear picture of the resulting free and forced vibrations, the amplitudes, the phase angles, the whirling motions, and the effects of damping for this simple shaft.

2. Review of Theory -- No Damping

(a) Equations of Motion

Consider a clamped-clamped, slender shaft rotating with a constant rotation speed Ω. For simplicity, the shaft will be represented by a concentrated disk of mass M located at the center of a flexible but weightless shaft as shown in Fig. 1. The shaft is represented as having a rectangular cross-

section so that the resulting elastic deflections q_η and q_ζ in the η and ζ directions at the center of shaft, can be more easily visualized. Also, there is an initial bow h_η and h_ζ at the center of the shaft. Rotation of the shaft is characterized by the angle $\psi = \Omega t$, while "whirling" motions of the shaft are characterized by vibrations of q_η and q_ζ which are near 90° out of phase with each other. The axes y and z pass through the two bearings and are fixed to ground, while the axes η and ζ pass through the center of the concentrated disk mass M and are fixed to it, so that they rotate with the disk mass. All torsional deflections and vibrations will be neglected in this analysis.

The absolute displacements of the disk C.G. are given by,

$$y_c = (q_\eta + h_\eta) \cos \psi - (q_\zeta + h_\zeta) \sin \psi$$

$$z_c = (q_\eta + h_\eta) \sin \psi + (q_\zeta + h_\zeta) \cos \psi \qquad (1)$$

The corresponding absolute velocities at the C.G. are,

$$\dot{y}_c = [\dot{q}_\eta - \Omega(q_\zeta + h_\zeta)] \cos \psi - [\dot{q}_\zeta + \Omega(q_\eta + h_\eta)] \sin \psi$$

$$\dot{z}_c = [\dot{q}_\eta - \Omega(q_\zeta + h_\zeta)] \sin \psi + [\dot{q}_\zeta + \Omega(q_\eta + h_\eta)] \cos \psi \qquad (2)$$

and the corresponding absolute accelerations at the C.G. are,

$$\ddot{y}_c = [\ddot{q}_\eta - 2\Omega\dot{q}_\zeta - \Omega^2(q_\eta + h_\eta)] \cos\psi$$

$$- [\ddot{q}_\zeta + 2\Omega\dot{q}_\zeta - \Omega^2(q_\zeta + h_\zeta)] \sin\psi \qquad (3)$$

$$\ddot{z}_c = [\ddot{q}_\eta - 2\Omega\dot{q}_\zeta - \Omega^2(q_\eta + h_\eta)] \sin\psi$$

$$+ [\ddot{q}_\zeta + 2\Omega\dot{q}_\eta - \Omega^2(q_\zeta + h_\zeta)q_\zeta] \cos\psi$$

The accelerations above can be resolved along the η and ζ directions to give the familiar accelerations in the rotating frame directions as,

$$\ddot{\eta}_c = \ddot{y}_c \cos\psi + \ddot{z}_c \sin\psi$$

$$= \ddot{q}_\eta - 2\Omega\dot{q}_\zeta + \Omega^2(q_\eta + h_\eta) \qquad (4)$$

$$\ddot{\zeta}_c = -\ddot{y}_c \sin\psi + \ddot{z}_c \cos\psi$$

$$= \ddot{q}_\zeta + 2\Omega\dot{q}_\eta - \Omega^2(q_\zeta + h_\zeta)$$

The equations of motion of the rotating disk are obtained by summing all forces acting on the disk in the η and ζ directions to give,

$$M\ddot{\eta}_c + k_\eta q_\eta + Mg \sin\psi = 0 \qquad (5)$$

$$M\ddot{\zeta}_c + k_\zeta q_\zeta + Mg \cos\psi = 0$$

where $k_\eta\, q_\eta$ and $k_\zeta\, q_\zeta$ are the spring forces due to shaft deflections and Mg represents a vertical acting gravity load on the disk. See Fig. 1. Substituting $\ddot{\eta}_c$ and ζ_c from Eqs. (4) into the above gives finally,

$$\begin{aligned} M\ddot{q}_\eta - 2\Omega M\dot{q}_\zeta + (k_\eta - M\Omega^2)q_\eta &= M\Omega^2 h_\eta - Mg \sin \Omega t \\ M\ddot{q}_\zeta + 2\Omega M\dot{q}_\eta + (k_\zeta - M\Omega^2)q_\zeta &= M\Omega^2 h_\zeta - Mg \cos \Omega t \end{aligned} \tag{6}$$

Equations (6) are the basic equations of motion for a slender, rotating, initially bowed shaft, subject to gravity forces, but neglecting damping. The $M\Omega^2 q$ and $2\Omega M\dot{q}$ terms represent the centrifugal and Coriolis forces respectively. These equations give the motion q_η and q_ζ relative to the rotating frame. The motion seen by a fixed ground observer y_c and z_c would be obtained by substituting the resulting q_η and q_ζ into Eqs. (1). Also, the forces acting at the bearings in the y and z directions would be given by

$$\begin{aligned} F_{BY} &= k_\eta\, q_\eta \cos \psi - k_\zeta\, q_\zeta \sin \psi \\ F_{BZ} &= k_\eta\, q_\eta \sin \psi + k_\zeta\, q_\zeta \cos \psi \end{aligned} \tag{7}$$

(b) Free Vibrations and Stability

To investigate the free vibrations and stability of the rotating shaft, one sets the right-hand-side of Eqs. (6) equal to zero to obtain the homogeneous equations,

$$\ddot{q}_\eta - 2\Omega\dot{q}_\zeta + (\omega_\eta^2 - \Omega^2)\, q_\eta = 0$$

$$\ddot{q}_\zeta + 2\Omega q_\eta + (\omega_\zeta^2 - \Omega^2)\, q_\zeta = 0 \qquad (8)$$

where $\omega_\eta = \sqrt{k_\eta/M}$ and $\omega_\zeta = \sqrt{k_\zeta/M}$ represent the natural frequencies of the shaft in the η and ζ directions respectively. Then assuming solutions of the form

$$q_\eta = \bar{q}_\eta\, e^{pt}, \qquad q_\zeta = \bar{q}_\zeta\, e^{pt} \qquad (9)$$

and setting the resulting determinant of Eqs. (8) equal to zero, one obtains the characteristic equation,

$$p^4 + (\omega_\eta^2 + \omega_\zeta^2 + 2\Omega^2)\, p^2 + (\omega_\eta^2 - \Omega^2)(\omega_\zeta^2 - \Omega^2) = 0 \qquad (10)$$

which can be readily solved to obtain the four characteristic roots p. For the common case of a circular (or square) cross-section shaft where $\omega_\eta = \omega_\zeta = \omega_N$, the solution of Eq. (10) is particularly simple and yields the four roots,

$$p = \pm\,(\omega_N + \Omega)i \quad , \qquad \pm\,(\omega_N - \Omega)i \qquad (11)$$

Since the roots are all imaginary, Eqs. (9) imply the natural frequencies of vibration ω_1 and ω_2 given as,

$$\omega_1 = \omega_N + \Omega$$

$$\omega_2 = \begin{cases} \omega_N - \Omega & \text{for} \quad 0 < \Omega < \omega_N \\ \Omega - \omega_N & \text{for} \quad \Omega > \omega_N \end{cases} \tag{12}$$

These frequencies are shown plotted in Fig. 2.

The corresponding motions q_η and q_ζ during these vibrations can be found by substituting Eqs. (9) into the second of Eqs. (8) to obtain,

$$\bar{q}_\zeta = \frac{-2\Omega p}{p^2 + \omega_N^2 - \Omega^2} \bar{q}_\eta \tag{13}$$

Setting arbitrarily $\bar{q}_\eta = C$ and introducing the roots p from Eq. (11) into the above gives $\bar{q}_\zeta = iC$ for ω_1, and $\bar{q}_\zeta = -iC$ for ω_2 when $0 < \Omega < \omega_N$, while $\bar{q}_\zeta = iC$ for ω_2 when $\Omega > \omega_N$. For the natural frequency ω_1, this implies the physical vibration motion,

$$q_\eta(t) = \text{Re}\left\{ Ce^{i\omega_1 t} \right\} = C \cos \omega_1 t$$

$$q_\zeta(t) = \text{Re}\left\{ iCe^{i\omega_1 t} \right\} = -C \sin \omega_1 t \tag{14}$$

which can be interpreted as a backward (clockwise) whirl motion of frequency ω_1 relative to the rotating shaft (see Fig. 1). In a similar way, the ω_2 natural frequency can be shown to appear as a forward whirl motion for

$0 < \Omega < \omega_N$, and as a backward whirl for $\Omega > \omega_N$, relative to the shaft. The motion seen by a fixed observer on the ground y_c and z_c for the ω_1 mode, would be obtained by substituting q_η and q_ζ from Eq. (14) into Eq. (1) to give,

$$y_c = C \cos \omega_N t + h \cos (\Omega t + \phi)$$

$$z_c = -C \sin \omega_N t + h \sin (\Omega t + \phi) \tag{15}$$

where $h = \sqrt{h_\eta^2 + h_\zeta^2}$ and ϕ is an arbitrary phase angle. The resultant motion is thus seen by a fixed observer as a forward whirl at frequency Ω caused by the initial bowing h, and a backward whirl at frequency ω_N caused by the free vibration. For small bowing ($h << C$), the motion appears as a backward whirl as in Eq. (14) only now, the frequency is ω_N rather than ω_1. Similarly, one can obtain the motion corresponding to the ω_2 vibration mode.

In the case of a non-circular (or non-square) cross-section shaft where $\omega_\eta \neq \omega_\zeta$, the general characteristic equation (Eq. (10) will yield a positive real root p between $\omega_\eta < \Omega < \omega_\zeta$, since the last term of the characteristic equation becomes negative in this interval. This positive real root indicates a static instability or divergence in this region. In reality, however, the static instability is limited by nonlinear bending effects to a large bowed-out position, rather than to infinite deflection. As the higher frequency ω_ζ approaches infinity, the region of static instability increases, and the system acts like an unstable single degree of freedom system instead of the two degree of freedom system described by Eqs. (6). It is interesting to note that for the circular (or square) cross-section shaft, the system never diverges.

(c) Forced Response

To investigate the forced response of the rotating shaft, one seeks particular solutions of Eqs. (6) in the form,

$$q_\eta(t) = q_{\eta 0} + A_s \sin \Omega t$$

$$q_\zeta(t) = q_{\zeta 0} + B_c \cos \Omega t \tag{16}$$

Placing these equations into Eqs. (6) and matching the constant, sine and cosine terms for each equation yields

$$(\omega_\eta^2 - \Omega^2)\, q_{\eta 0} = \Omega^2 h_\eta$$

$$(\omega_\zeta^2 - \Omega^2)\, q_{\zeta 0} = \Omega^2 h_\zeta$$

$$(\omega_\eta^2 - 2\Omega^2)\, A_s + 2\Omega^2\, B_c = -g \tag{17}$$

$$2\Omega^2 A_s + (\omega_\zeta^2 - 2\Omega^2)\, B_c = -g$$

For the common case of a circular (or square) cross-section shaft where $\omega_\eta = \omega_\zeta = \omega_N$, these equations can be solved simply to give,

$$q_{\eta 0} = \frac{\Omega^2}{\omega_N^2 - \Omega^2} h_\eta \quad , \qquad q_{\zeta 0} = \frac{\Omega^2}{\omega_N^2 - \Omega^2} h_\zeta$$

$$A_s = B_c = -\frac{g}{\omega_N^2} \tag{18}$$

Substituting these back into Eqs. (16) gives the forced response of the shaft as,

$$q_\eta = \frac{\Omega^2}{\omega_N^2 - \Omega^2} h_\eta - \frac{g}{\omega_N^2} \sin \Omega t$$

$$q_\zeta = \frac{\Omega^2}{\omega_N^2 - \Omega^2} h_\zeta - \frac{g}{\omega_N^2} \cos \Omega t \qquad (19)$$

The first term in the above equations represents the effect of initial bowing h_η, h_ζ, and it bows out the shaft statically more and more as the rotation speed Ω increases until at the critical speed $\Omega = \omega_N$, it theoretically goes to infinity. Beyond $\Omega = \omega_N$, the deflections q_η and q_ζ come back on the negative side and approach the limits $-h_\eta$ and $-h_\zeta$ respectively, thus demonstrating the well known "self-centering" effect of super critical rotors. See Figs. 3 and 1. The second term in Eqs. (19) represents the effect of the gravity loads, and according to the simple linear theory assumed here, it results in a constant amplitude oscillating deflection of the rotating shaft of magnitude $g/\omega_N^2 = Mg/k$, up to and beyond the critical speed $\Omega = \omega_N$.

The motion seen by a fixed observer on the ground y_c and z_c would be obtained by substituting q_η and q_ζ from Eq. (19) back into Eq. (1), and would result in,

$$y_c = \frac{\omega_N^2}{\omega_N^2 - \Omega^2} h \cos (\Omega t + \phi)$$

$$z_c = \frac{\omega_N^2}{\omega_N^2 - \Omega^2} h \sin (\Omega t + \phi) - \frac{g}{\omega_N^2} \qquad (20)$$

where,

$$h \equiv \sqrt{h_\eta^2 + h_\zeta^2}$$

$$\tan \phi = h_\zeta / h_\eta \tag{21}$$

This represents a forward whirling motion at frequency Ω and of observed amplitude,

$$A_{OB} = \frac{\omega_N^2}{\omega_N^2 - \Omega^2} \, h \tag{22}$$

superimposed on a steady downward deflection, g/ω_N^2. This again illustrates the "self-centering" effect of supercritical rotors.

The force transmitted to the bearings in the y and z directions can be formed by substituting Eqs. (19) into Eqs. (7). For this circular cross-section beam, the forces become,

$$F_{BY} = k \frac{\Omega^2}{\omega_N^2 - \Omega^2} \, h \cos (\Omega t + \phi)$$

$$F_{BZ} = k \frac{\Omega^2}{\omega_N^2 - \Omega^2} \, h \sin (\Omega t + \phi) - Mg \tag{23}$$

Comparing Eqs. (23) with (19), it should be noted that the bearings feel an oscillating force due to the bowing and a constant force due to gravity, while the rotating shaft feels a constant force due to the bowing and an oscillatory force due to gravity.

3. Review of Theory -- Effect of Damping

(a) Equations of Motion

The previous results are modified somewhat by the presence of damping. For the slender shafts here, two main types of damping will be considered, namely, structural damping of the shaft and air damping. Another type, bearing damping acts somewhat similarly to air damping.

The structural damping is due to internal motions of the shaft, and is characterized by forces proportional to the shaft relative velocities as $c_{s\eta}\ \dot{q}_\eta$ and $c_{s\zeta}\ \dot{q}_\zeta$, while the aerodynamic and bearing damping is due to external motions of the shaft and is characterized by forces proportional to the shaft absolute velocities as $c_{Ay}\ \dot{y}_c$ and $c_{Az}\ \dot{z}_c$. It will be assumed further, that all dampings are isotropic so that $c_{s\eta} = c_{s\zeta} = c_s$ and $c_{Ay} = c_{Az} = c_A$. The total damping forces along the η and ζ directions (see Fig. 1), can then be expressed as,

$$F_{\eta D} = -c_s\ \dot{q}_\eta - c_A\ \dot{y}_c \cos\psi - c_A\ \dot{z}_c \sin\psi$$

$$F_{\zeta D} = -c_s\ \dot{q}_\zeta + c_A\ \dot{y}_c \sin\psi - c_A\ \dot{z}_c \cos\psi \qquad (24)$$

Substituting $\dot{y}_c$ and $\dot{z}_c$ from Eqs. (2) into the above gives the damping forces as,

$$F_{\eta D} = -c_s\ \dot{q}_\eta - c_A\ [\dot{q}_\eta - \Omega(q_\zeta + h_\zeta)]$$

$$F_{\zeta D} = -c_s\ \dot{q}_\zeta - c_A\ [\dot{q}_\zeta + \Omega(q_\eta + h_\eta)] \qquad (25)$$

It is to be noted that the aerodynamic damping here is proportional to displacements q_η, q_ζ as well as to the velocities $\dot{q}_\eta$, $\dot{q}_\zeta$.

Equations (25) are added to the right-hand-sides of Eqs. (6) to provide the effect of damping. Upon assuming a circular shaft ($\omega_\eta = \omega_\zeta = \omega_N$) and dividing through by the mass M, one obtains,

$$\ddot{q}_\eta + 2(\zeta_s + \zeta_A)\,\omega_N\,\dot{q}_\eta - 2\Omega\dot{q}_\zeta + (\omega_N^2 - \Omega^2)\,q_\eta - 2\zeta_A\omega_N\Omega q_\zeta$$

$$= \Omega^2 h_\eta + 2\zeta_A\omega_N\Omega h_\zeta - g \sin \Omega t$$

$$\ddot{q}_\zeta + 2(\zeta_s + \zeta_A)\,\omega_N\,\dot{q}_\zeta + 2\Omega\dot{q}_\eta + (\omega_N^2 - \Omega^2)\,q_\zeta + 2\zeta_A\omega_N\Omega q_\eta$$

$$= \Omega^2 h_\zeta - 2\zeta_A\omega_N\Omega h_\eta - g \cos \Omega t \qquad (26)$$

where one has introduced the critical damping ratios $\zeta_s = c_s/2\omega_N M$ and $\zeta_A = c_A/2\omega_N M$ for convenience. Equations (26) are the basic equations for investigating the effects of damping on a slender, rotating, initially bowed shaft, subject to gravity forces.

(b) Free Vibrations and Stability

To investigate for free vibrations and stability, one again sets the right-hand-side of Eqs. (26) equal to zero, and assumes solutions of the form of Eq. (9). Then setting the resulting determinant equal to zero, one obtains the fourth order characteristic equation,

$$[p^2 + 2(\zeta_s + \zeta_A)\,\omega_N p + (\omega_N^2 - \Omega^2)]^2 + [2\Omega p + 2\zeta_A\omega_N\Omega]^2 = 0 \qquad (27)$$

which can be factored into two complex second order factors,

$$p^2 + [2(\zeta_s + \zeta_A)\,\omega_N + i2\Omega]\,p + [\omega_N^2 - \Omega^2 + i2\zeta_A\omega_N\Omega] = 0$$

$$p^2 + [2(\zeta_s + \zeta_A)\,\omega_N - i2\Omega]\,p + [\omega_N^2 - \Omega^2 - i2\zeta_A\omega_N\Omega] = 0 \qquad (28)$$

Looking at the first factor, one can solve for p to obtain

$$p = -(\zeta_s + \zeta_A)\,\omega_N - i\Omega \pm \sqrt{-\omega_N^2\,[1 - (\zeta_s + \zeta_A)^2] + i2\Omega\omega_N\zeta_s} \qquad (29)$$

This can be simplified by using the identity,

$$\sqrt{A + Bi} = \pm\,(C + Di)$$

$$D = \sqrt{\sqrt{A^2 + B^2} - A}\,\Big/\sqrt{2}\,, \quad C = B/2D \qquad (30)$$

and then assuming small damping ζ_s, $\zeta_A \ll 1$, to obtain two of the four roots p of the characteristic Eq. (27). Similarly, the second factor of Eq. (28) can be solved to give two additional roots p. These four characteristic roots of Eq. (27) are,

$$p \approx [-(\zeta_s + \zeta_A)\,\omega_N - \zeta_s\Omega] \pm (\omega_N + \Omega)i$$

$$p \approx [-(\zeta_s + \zeta_A)\,\omega_N + \zeta_s\Omega] \pm (\omega_N - \Omega)i \qquad (31)$$

These roots are compared with the previous pure imaginary roots Eqs. (11) for the undamped system. The frequencies are seen to be the same (because of the ζ_s, $\zeta_A << 1$ assumption), but now there are real parts present. The damping associated with each of the two frequencies ω_1 and ω_2 of Fig. 2 are then,

$$\begin{aligned} \omega_1 &\rightarrow [-(\zeta_s + \zeta_A)\,\omega_N - \zeta_s\Omega] \\ \omega_2 &\rightarrow [-(\zeta_s + \zeta_A)\,\omega_N + \zeta_s\Omega] \end{aligned} \tag{32}$$

It is seen that the ω_1 frequency mode becomes increasingly greater damped as the rotation speed Ω increases, but the ω_2 mode decreases in damping until above some critical speed Ω_{cr}, the shaft becomes dynamically unstable. This critical speed is found from Eq. (32) to be,

$$\Omega_{cr} = \left(\frac{\zeta_s + \zeta_A}{\zeta_s} \right) \omega_N \tag{33}$$

and is seen to depend on the ratio of structural to aerodynamic and bearing damping.

It should be mentioned that in the vicinity of $\Omega \approx \omega_N$, the assumption of ζ_s, $\zeta_A << 1$ has to be applied with caution for the ω_2 frequency mode. In this case, the solution of Eqs. (29) and (30) would not lead to exactly $\omega_2 = 0$, but rather to a small finite value for ω_2. In fact, at $\Omega = \omega_N$, Eqs. (29) and (30) would yield the frequency,

$$\omega_2 \approx \frac{1}{2} [(\zeta_s + \zeta_A)^2 - \zeta_s^2]\, \omega_N \tag{34}$$

rather than $\omega_2 = 0$.

The mode shapes during the damped vibrations can be obtained similarly to that for the undamped case, and will result in similar type modes.

(c) Forced Response

To investigate the forced response of the damped rotating shaft, it is convenient to seek particular solutions of Eqs. (26) in the form,

$$q_\eta(t) = q_{\eta 0} + \bar{q}_\eta \, e^{i\Omega t}$$
$$q_\zeta(t) = q_{\zeta 0} + \bar{q}_\zeta \, e^{i\Omega t} \tag{35}$$

Placing these solutions into Eqs. (26), treating the g sin Ωt and g cos Ωt terms as the real parts of -g i $e^{\Omega t}$ and g $e^{\Omega t}$ respectively, and matching the constant and $e^{i\Omega t}$ terms of each equation gives

$$(\omega_N^2 - \Omega^2)\, q_{\eta 0} - 2\zeta_A \omega_N \Omega q_{\zeta 0} = \Omega^2 h_\eta + 2\zeta_A \omega_N \Omega h_\zeta$$

$$2\zeta_A \omega_N \Omega q_{\eta 0} + (\omega_N^2 - \Omega^2) q_{\zeta 0} = \Omega^2 h_\zeta - 2\zeta_A \omega_N \Omega h_\eta$$

$$[2(\zeta_s + \zeta_A)\, \omega_N \Omega i + (\omega_N^2 - 2\Omega^2)]\, \bar{q}_\eta + [-2\Omega^2 i - 2\zeta_A \omega_N \Omega]\, \bar{q}_\zeta = ig$$

$$[2\Omega^2 i + 2\zeta_A \omega_N \Omega]\, \bar{q}_\eta + [2(\zeta_s + \zeta_A)\, \omega_N \Omega i + (\omega_N^2 - 2\Omega^2)]\, \bar{q}_\zeta = -g \tag{36}$$

The first two equations above involving the constant terms $q_{\eta 0}$ and $q_{\zeta 0}$, can be solved to give,

$$q_{\eta 0} = \frac{[(\omega_N^2 - \Omega^2)\,\Omega^2 - (2\zeta_A \omega_N \Omega)^2]\, h_\eta + [2\zeta_A \omega_N^3 \Omega]\, h_\zeta}{(\omega_N^2 - \Omega^2)^2 + (2\zeta_A \omega_N \Omega)^2}$$

$$q_{\zeta 0} = \frac{[(\omega_N^2 - \Omega^2)\,\Omega^2 - (2\zeta_A \omega_N \Omega)^2]\, h_\zeta - [2\zeta_A \omega_N^3 \Omega]\, h_\eta}{(\omega_N^2 - \Omega^2)^2 + (2\zeta_A \omega_N \Omega)^2} \tag{37}$$

The second two equations of Eqs. (36) can also be solved for $\bar{q}_\eta$ and q_ζ after some algebra and using the same factoring scheme of Eqs. (27) and (28) to obtain simply,

$$\bar{q}_\eta = \frac{i\, g}{\omega_N^2 + 2\zeta_s \omega_N \Omega i}, \qquad \bar{q}_\zeta = \frac{-g}{\omega_N^2 + 2\zeta_s \omega_N \Omega i} \tag{38}$$

Substituting these $\bar{q}_\eta$ and $\bar{q}_\zeta$ back into Eqs. (35) and then taking the real part of the resulting equations, gives the final physical forced response of the shaft as,

$$q_\eta = q_{\eta 0} - \frac{g}{\omega_N \sqrt{\omega_N^2 + (2\zeta_s \Omega)^2}} \sin(\Omega t - \gamma)$$

$$q_\zeta = q_{\zeta 0} - \frac{g}{\omega_N \sqrt{\omega_N^2 + (2\zeta_s \Omega)^2}} \cos(\Omega t - \gamma) \tag{39}$$

where,

$$\tan \gamma = 2\zeta_s \Omega/\omega_N \tag{40}$$

and $q_{\eta 0}$ and $q_{\zeta 0}$ are given by Eqs. (37). The above solution is to be compared with the no damping case Eqs. (19) determined previously. Again, the first term represents the static effect of initial bowing, while the second term represents the oscillatory effect of the gravity load.

Regarding the static effect of the initial bowing, the maximum static deflection for small damping occurs at $\Omega \approx \omega_N$. From Eqs. (37), this results in the maximum deflections,

$$(q_{\eta 0})_{max} = \frac{h_\zeta}{2\zeta_A} - h_\eta \quad , \quad (q_{\zeta 0})_{max} = -\frac{h_\eta}{2\zeta_A} - h_\zeta \tag{41}$$

at resonance. It is interesting to note that the static deflection of the shaft $q_{\eta 0}$ and $q_{\zeta 0}$ is strongly influenced by the aerodynamic (and bearing) damping ζ_A present in the system. In fact, this damping prevents the shaft from bowing out to infinity as indicated by the no damping solution, Eq. (19), during passage through the critical speed, $\Omega = \omega_N$. An example of the bowed-out position of the shaft, $q_{\eta 0}$ and $q_{\zeta 0}$ versus rotation speed Ω, is shown in Fig. 3 for a typical shaft with an aerodynamic critical damping ratio, $\zeta_A = .014$. It should be noted that $q_{\eta 0}$ and $q_{\zeta 0}$ do not pass through zero at the same frequency, but the total static deflection given by $q_0 = \sqrt{q_{\eta 0}^2 + q_{\zeta 0}^2}$ becomes a maximum at $\Omega \approx \omega_N$. This passage through the critical speed is easier visualized by the polar plot of shaft deflection given in Fig. 4.

Regarding the effect of the gravity load, it can be seen from Eqs. (39) that the oscillatory amplitude depends only on the structural damping ζ_s, and that it decreases very slowly with rotation speed Ω. In fact, for small structural damping ζ_s, the amplitude remains almost constant as in the no-damping case.

The motion seen by a fixed observer on the ground y_c and z_c is again found by substituting q_η and q_ζ from Eq. (39) into Eq. (1) and results, after some algebra, in the following,

$$y_c = A_{OB} \cos(\Omega t + \phi) + \frac{g \sin\gamma}{\omega_N \sqrt{\omega_N^2 + (2\zeta_2\Omega)^2}}$$

$$z_c = A_{OB} \sin(\Omega t + \phi) - \frac{g \cos\gamma}{\omega_N \sqrt{\omega_N^2 + (2\zeta_s\Omega)^2}} \tag{42}$$

where one now has,

$$A_{OB} = \frac{\omega_N^2}{\sqrt{(\omega_N^2 - \Omega^2)^2 + (2\zeta_A\omega_N\Omega)^2}}\, h \tag{43}$$

$$\tan\phi = \frac{(\omega_N^2 - \Omega^2)\, h_\zeta - 2\zeta_A\omega_N\Omega h_\eta}{(\omega_N^2 - \Omega^2)\, h_\eta + 2\zeta_A\omega_N\Omega h_\zeta} \tag{44}$$

and h is the total initial bow given by Eq. (21) while γ is defined previously in Eq. (40). These results are to be compared with the no damping solutions, Eqs. (20). They again represent a foward whirling motion at frequency Ω, superimposed on a steady downward gravity deflection which is now shifted forward slightly because of the structural damping ζ_s contained in γ. Figure 5 shows an example of the observed amplitude A_{OB} versus rotational speed Ω for a typical shaft with an aerodynamic damping ratio $\zeta_A = .014$. The maximum amplitude is seen to occur at $\Omega \approx \omega_N$ and is given from Eq. (43) simply as,

$$(A_{OB})_{max} = \frac{h}{2\zeta_A} \tag{45}$$

This is what an observer would see for the shaft at its critical resonance speed.

4. Experiment

An experiment was performed to examine the basic theoretical behavior described in the previous sections. The experiment was set up and run by the latter two authors as part of an experimental project. Some previous initial work had also been done by another student, Stephen Levin.

The test bed set-up consisted basically of a motor driven shaft assembly, See Fig. 6. The steel channel frame supporting the shaft was .152 m (6 in.) wide, 1.829 m (6 ft.) long, and was secured to the test-bed with C-clamps. A variable speed motor with a range of 0 to 48 Hz was mounted on the test-bed next to the end of the frame, and was connected to the slip ring assembly by a flexible coupling. One end of the test shaft was inserted into a tight

fitting bushing on the slip ring assembly, while the other end was supported by two ball bearings separated a few inches apart. This design simulated clamped-clamped end conditions.

The shaft was made of 6.35 mm (1/4 in.) diameter aluminum 2024 rod, and had a length of 1.334 m (52.5 in.) between the clamped ends. An aluminum flywheel with a single slit on its edge was attached to the shaft between the two end bearings. The slit passed through an optic sensor and gave a short pulse for each revolution, which could be counted by a frequency counter to give the rotation speed. Four strain gages were placed 90° apart around the shaft at the end near the slip ring assembly. The strain signals were taken out by the slip rings and viewed on an oscilloscope to provide an indication of shaft bending in two perpendicular directions. Also, both strain gage signals and the optic sensor pulses were recorded on a Gould direct writing recorder oscillograph so that a permanent record could be made of the test runs.

The testing procedure was as follows. First, before starting the motor, the natural frequency of the shaft was determined by tapping the shaft in the center and recording the resulting vibrations on the oscillograph recorder. This also gave a measure of the damping of the system. Second, the shaft was rotated very slowly and an oscillograph record was taken. From the recorded sinusoidal amplitude of the strain gage traces and from the calculated deflection of the clamped shaft under uniform gravity loading, the center deflection of the shaft could be approximately calibrated. Next, the dynamic testing was done. The motor was rotated from zero to maximum rotation speed (48 Hz) and back down again, and a continuous oscillograph reading was taken. This was

done several times until the amplification levels on the oscillograph recorder were set properly. After that, detailed oscillograph readings were taken at several interesting frequencies, usually at and around resonance. Concurrently, independent visual observations of the bowed-out amplitude of the shaft were also taken by viewing the rotating, bowed-out shaft against a scale placed under it. Finally, at the end of the run, the slow rotation calibration test and the non-rotating natural frequency and damping test were repeated as a check on the earlier tests at the beginning of the run.

5. Results and Discussion

The first and second natural frequencies of the clamped-clamped shaft were estimated from the expressions,

$$\omega_1 = 22.0 \sqrt{EI/m\ell^4}$$

$$\omega_2 = 61.7 \sqrt{EI/m\ell^4} \qquad (46)$$

Using $E = 72.5 \times 10^9$ N/m^2 (10.5×10^6 lbs/in^2) and a mass per unit length $m = .0877$ Kg/m ($.1272 \times 10^{-4}$ lb-sec^2/in^2) for this .00635 m (1/4 in) diameter aluminum shaft, gave theoretical natural frequencies of $\omega_1 = 16.0$ Hz and $\omega_2 = 44.8$ Hz. These compared reasonably with the measured frequencies from transient decay tap tests of $\omega_1 = 15.0$ Hz and $\omega_2 = 41$ Hz. The slightly lower measured frequencies were probably due to not completely fixed end conditions.

The corresponding critical damping ratio for the lowest natural frequency ω_N = 15.0 Hz was measured from these transient decay tests as ζ = .015 approximately. Of this, the structural damping was estimated from the material properties to be $\zeta_S \approx .001$ while the aerodynamic and bearing damping accounted for the remainder and was taken to be $\zeta_A \approx .014$.

As mentioned previously, the static calibration of the shaft strain gage traces was evaluated by rotating the shaft slowly, noting the resulting sinusoidal oscillograph traces, and using the theoretical center deflection δ_c of a clamped beam under uniform gravity loading, namely,

$$\delta_c = \frac{mg\ell^4}{384\ EI} \tag{47}$$

where g is the acceleration of gravity.

Figure 7 shows a photograph of the shaft rotating close to its lowest critical speed, $\Omega \approx$ 15.0 Hz. The large bowed position of the shaft is apparent.

Figure 8 shows the strain gage traces q_ζ and q_η as the rotation speed is increased steadily from slow speeds up to and beyond the lowest critical speed of the shaft. Throughout this range, the amplitude of the gravity load oscillations remains more or less constant as indicated by theory, Eqs. (38), except for some small increases near the critical speed of the shaft. The static position of the traces $q_{\zeta 0}$ and $q_{\eta 0}$, however, change considerably as resonance is approached and reach peak values near there. It should be noted that $q_{\zeta 0}$ and $q_{\eta 0}$ do not pass through zero nor peak at the same frequency, which agrees with the theoretical calculations shown in Fig. 3. During a fast

passage through resonance, a rapid increase, then a rapid decrease in static deflection occurs which causes a backward whirl transient impulse on the shaft (see the polar plot, Fig. 4). This transient impulse is sufficient to excite the low frequency backward whirl vibration mode ω_2 indicated in Fig. 2. A more detailed look at this excitation is shown in Fig. 9 where the frequency sweep-through has been repeated using a faster oscillograph paper speed. The obvious 90° phase shift between the two traces is apparent and gives a clear picture of the backward whirl mode ω_2 whose frequency varies from 1.4 Hz at Ω = 16.4 Hz to 4.3 Hz at Ω = 19.2 Hz. These experimental points are shown plotted nondimensionally in Fig. 2.

Figure 10 shows a corresponding frequency sweep when Ω decreases through the resonance range. In this case, the ω_2 mode excited is now a forward whirl mode whose frequency varies from 1.5 Hz at Ω = 13.5 Hz to 2.9 Hz at Ω = 12.0 Hz. These points are also shown nondimensionally in Fig. 2.

The experimental center deflections q_ζ and q_η shown in Fig. 3 were determined from the strain gage traces as described earlier. These experimental points in Fig. 3 were obtained by dwelling at a given fixed rotation speed rather than from the frequency sweeps indicated in Figs. 8, 9, and 10. Experimental results seem to agree well with linear theory, using h = 1 mm and ζ_A = .014 (h_η and h_ζ were subsequently deduced for best fit of experimental data).

The experimental amplitude observed by a fixed observer A_{OB} is shown in Fig. 5 together with the theoretical estimates. These experimental points were obtained by independent visual observation while dwelling at a fixed rotation speed. Again, good correlation is obtained with linear theory. In

particular, Eq. (45) together with the measured values of $h \approx 1$ mm and $\zeta_A \approx .014$ gave good estimates of the observed maximum amplitudes at resonance here.

In addition to the first critical speed at $\Omega = 15$ Hz shown here, the second critical speed at $\Omega = 42$ Hz was also determined experimentally. Figure 11 shows a photograph of this resonance, and the second vibration mode is apparent. Similar static deflection displacement shifts in q_ζ and q_η occurred as in the neighborhood of the first critical speed resonance. This could be analyzed in a similar way using a more accurate distributed mass modal representation of the shaft instead of the simple concentrated mass model shown in Fig. 1.

Also, it should be mentioned in these experiments, a small subharmonic resonance of order 2 was found in the shaft at $\Omega \approx 30$ Hz. This is shown by the strain gage traces in Fig. 12 and indicates the center of the shaft is vibrating in a backward whirl mode at $\omega \approx 15$ Hz relative to the shaft ends, while the shaft ends were rotating at $\Omega \approx 30$ Hz. The phenomenon was also observed visually by a fixed observer. This indicates perhaps some nonlinear mechanism associated with shaft shortening or some parametric excitation is also ocurring. It should be noted that Eqs. (6) indicate that at $\Omega = 2\omega_N$, there is a natural frequency $\omega_2 = \omega_N = \Omega/2$. See Fig. 2.

6. Conclusions

The simple linear theory of slender rotating shafts has been reviewed for both free and forced vibrations. The role of external (aerodynamic and bearing) damping, internal (structural) damping, and various whirling and resonance phenomena have been explicitly indicated.

A simple experiment on a slender rotating shaft clearly revealed the various features of the linear theory for both free and forced vibrations. Good agreement was obtained between theory and experiment.

The detailed behavior of passing through the lowest critical speed was explicitly shown both theoretically and experimentally. The maximum static bowed-out deflection of the shaft at the critical speed was dependent on the aerodynamic and bearing damping present, and the initial bowing of the shaft. Simple expressions, Eqs. (41) and (45) estimated the maximum deflections achieved.

The oscillatory deflection of the shaft due to gravity loads remained more or less of constant amplitude except for some small increases near the critical speed of the shaft. However, these increases were small compared to the large static deflection of the shaft there.

During a rapid passage through the critical speed, the low frequency whirl mode ω_2 was readily excited transiently. This was clearly shown to be either a backward whirl or a forward whirl relative to the rotating shaft, depending on whether the rotation speed Ω was increased or was decreased through the critical speed. This lower free vibration mode ω_2 agreed well with the theoretical estimates given in Fig. 2.

At rotation speeds above the first critical speed $\Omega = \omega_N$, the shaft would appear to run smoothly, and showed the well known "self-centering" effect of supercritical shafts. However, large shaft deflections would occur again as the rotation speed Ω approached the second vibration mode of the shaft. Also, significant backward whirl vibrations of the first mode could be excited subharmonically when the rotation speed Ω approached twice the first mode natural frequency.

The preceding observations relative to the higher shaft vibration modes and to subharmonic excitation of the first mode could be explored further by using a more complex modal model of the shaft and including nonlinear effects. Also, further investigations could be made into questions of C.G. offsets, noncircular cross-sections, bearing motions, bearing damping, nonlinear effects, parametric excitation effects, and torsional oscillations of the shaft. It is hoped the present investigation has helped clarify some of the simpler linear aspects of slender rotating shaft vibrations.

References

1. Den Hartog, J.P., "Mechanical Vibrations", 4th Ed., McGraw-Hill Book Co., New York, 1956, Chap. 6.

2. Bolotin, V.V., "Nonconservative Problems of the Theory of Elastic Stability", MacMillan Co., New York, 1963, Chap. 3.

3. Ziegler, Hans, "Principles of Structural Stability", Blaisdell Publishing Co., Waltham, Massachusetts, 1968, Secs. 1.3, 3.2, 4.2.

4. Vance, J.M. and Royal, A.C., "High-Speed Rotor Dynamics - An Assessment of Current Technology for Small Turboshaft Engines", J. of Aircraft, Vol. 12, No. 4, April 1975, pp. 295-305.

5. Gunter, E.J., Jr., "Dynamic Stability of Rotor-Bearing Systems", NASA SP-113, 1966.

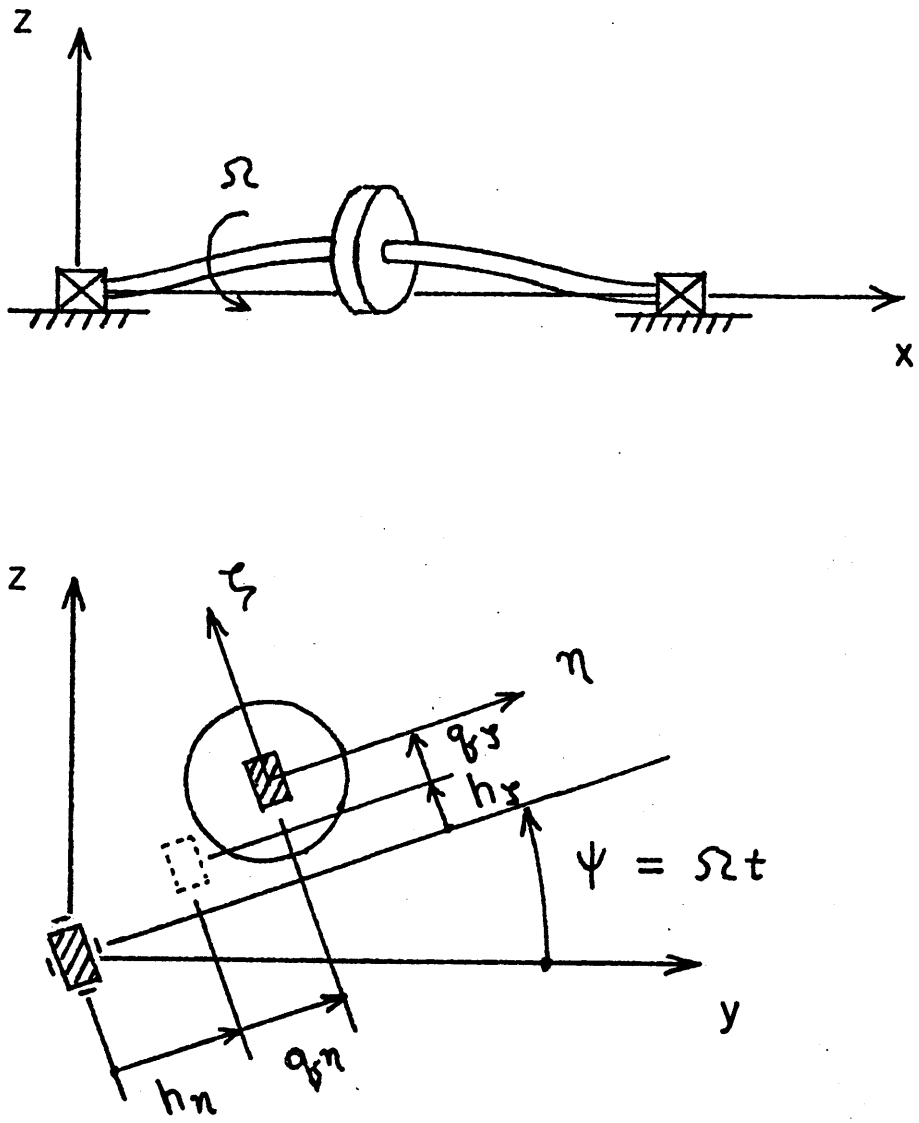

FIG. 1 ROTATING BEAM WITH CONCENTRATED DISK MASS

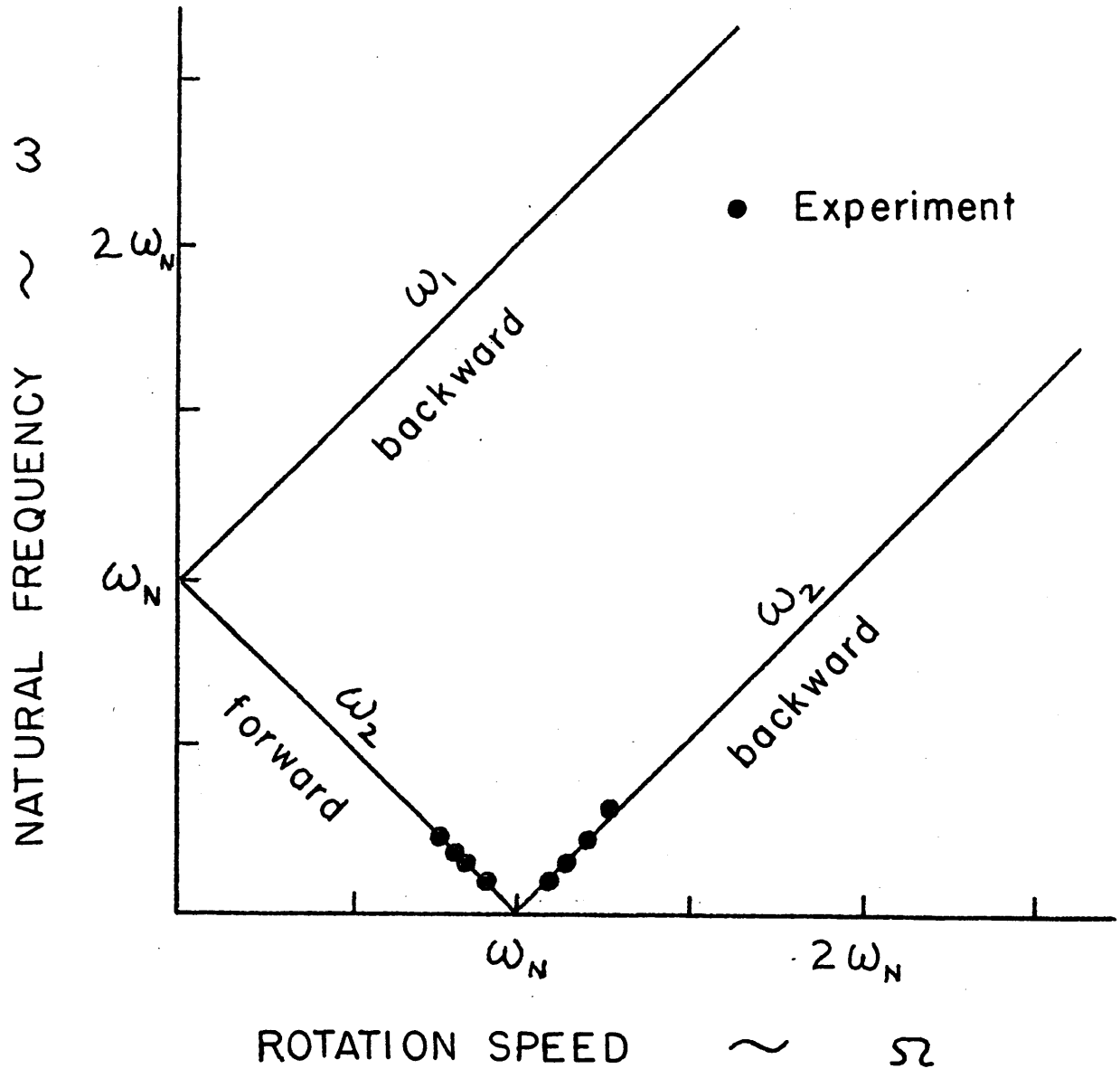

FIG. 2 FREQUENCIES OF FREE VIBRATIONS RELATIVE TO ROTATING SHAFT. NO DAMPING, $\omega_\eta = \omega_\zeta = \omega_N$. FOR EXPERIMENT, ω_N = 15.0 HZ

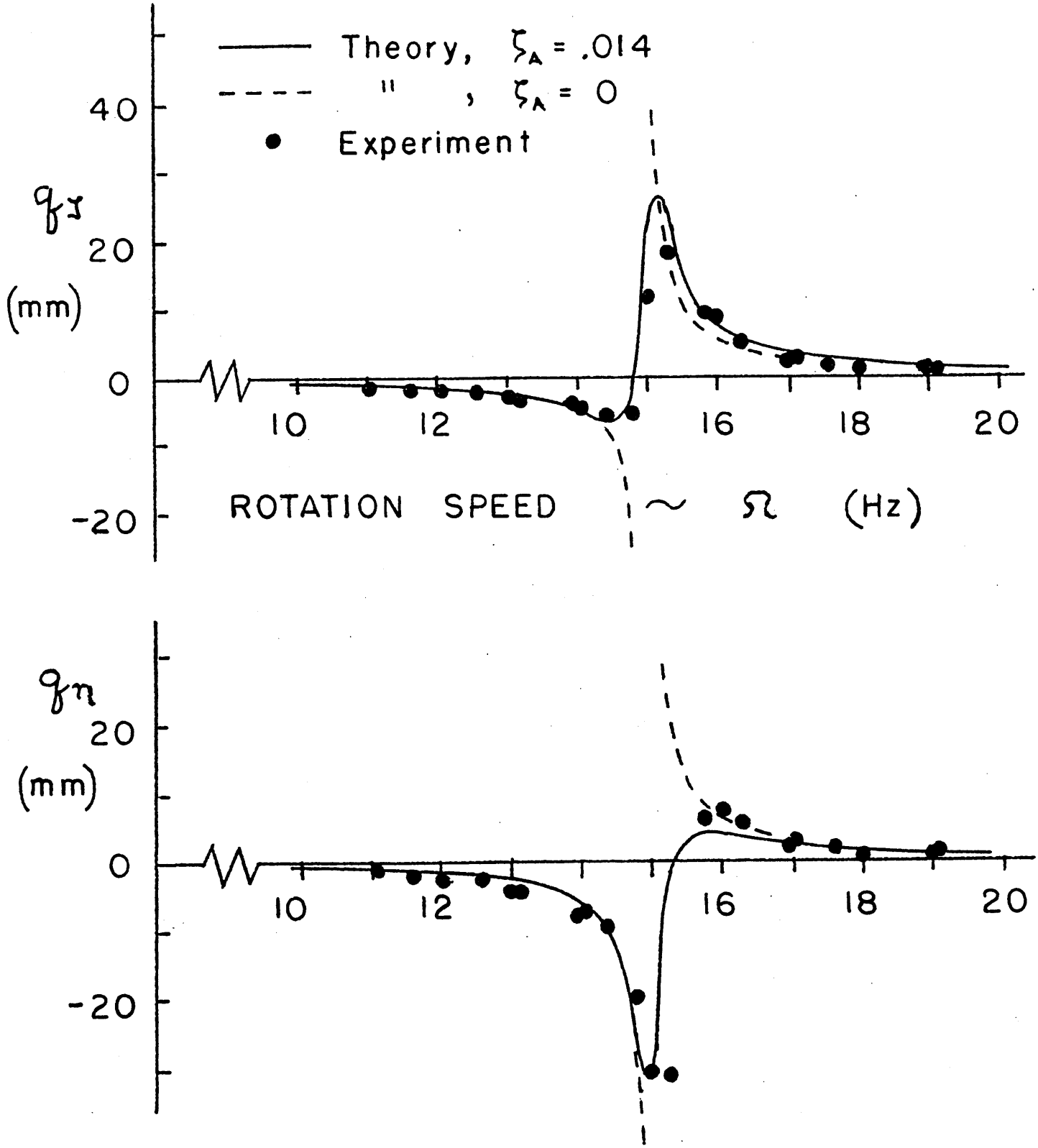

FIG. 3 STATIC DEFLECTION OF SHAFT DURING ROTATION. ω_N = 15.0 HZ, h_ξ = -.6 mm, h_η = -.8 mm

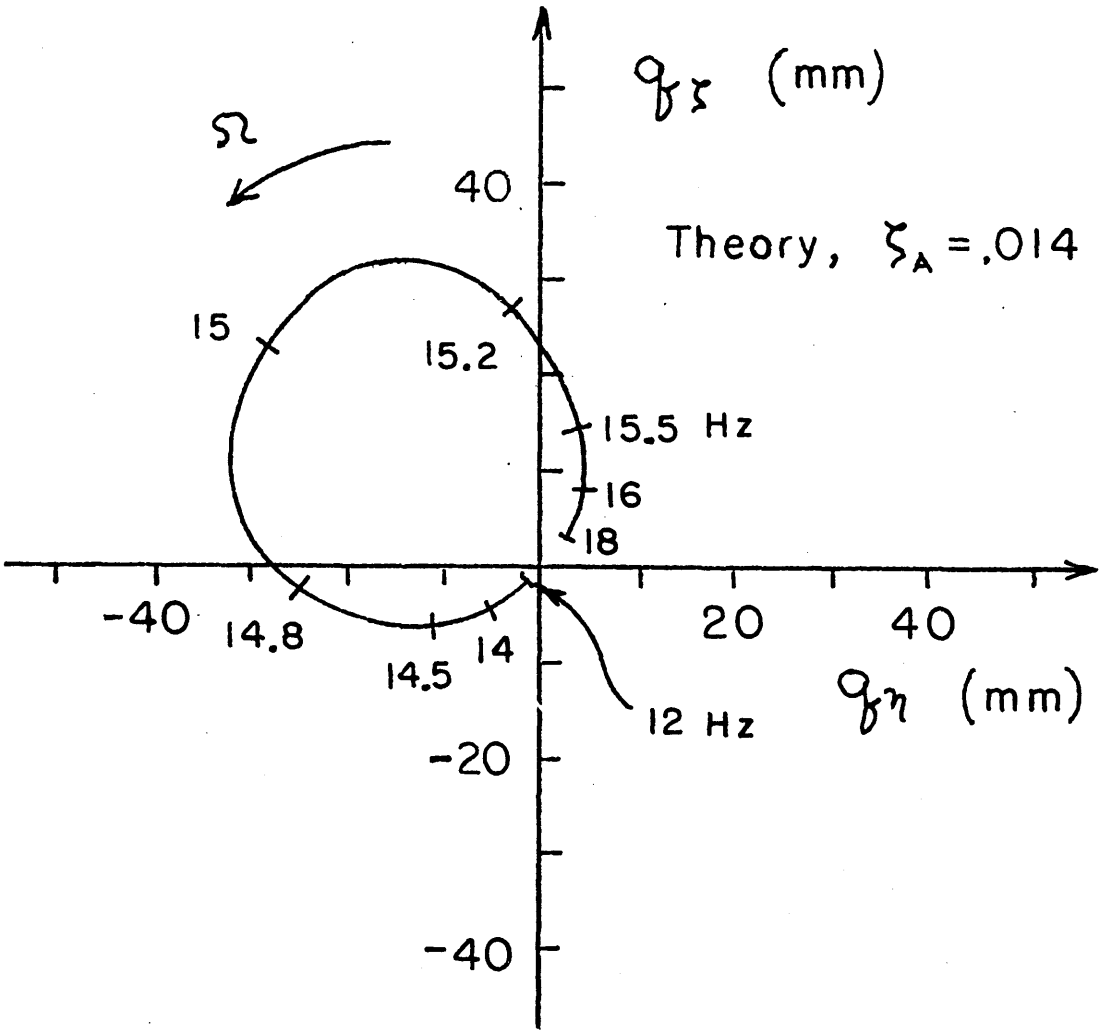

FIG. 4 POLAR PLOT OF STATIC DEFLECTION OF SHAFT NEAR CRITICAL SPEED.

ω_N = 15.0 HZ, h_ζ = -.6 mm, h_η = -.8 mm

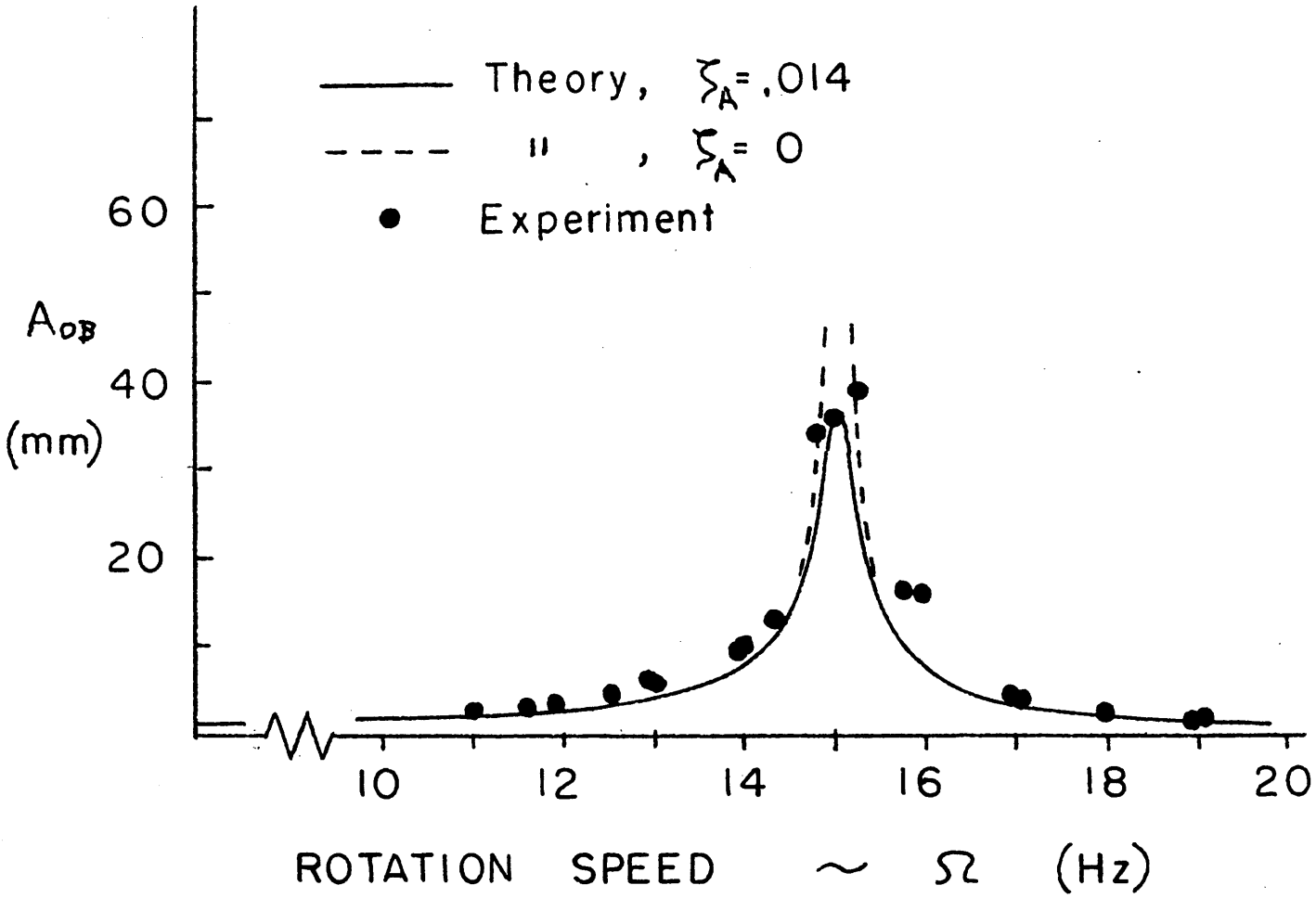

FIG. 5 AMPLITUDE OF SHAFT SEEN BY A FIXED OBSERVER DURING ROTATION.

ω_N = 15.0 HZ, h_ζ = -.6 mm, h_η = -.8 mm

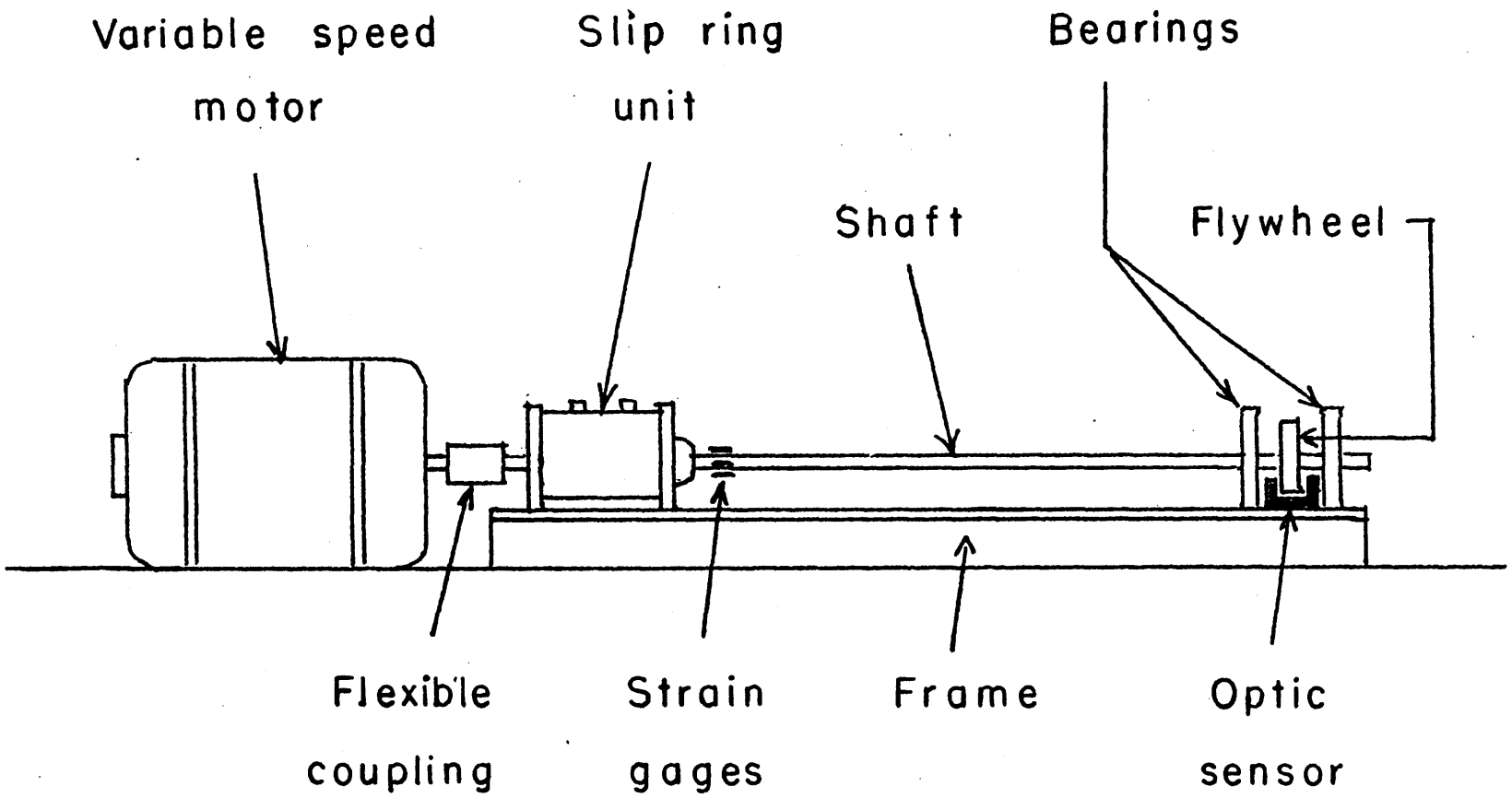

FIG. 6 LAYOUT OF EXPERIMENTAL TEST

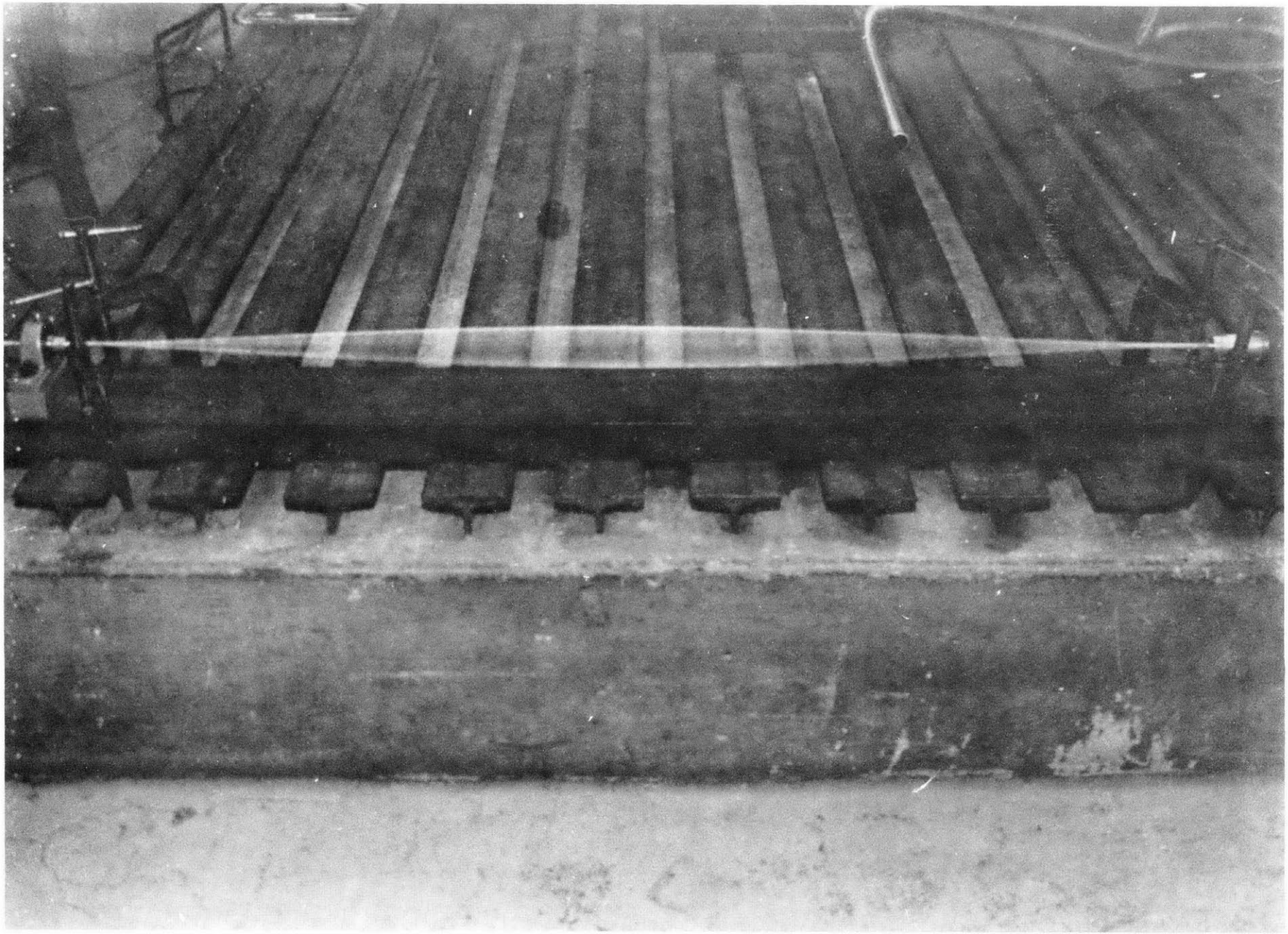

FIG. 7 SHAFT ROTATING AT FIRST CRITICAL SPEED

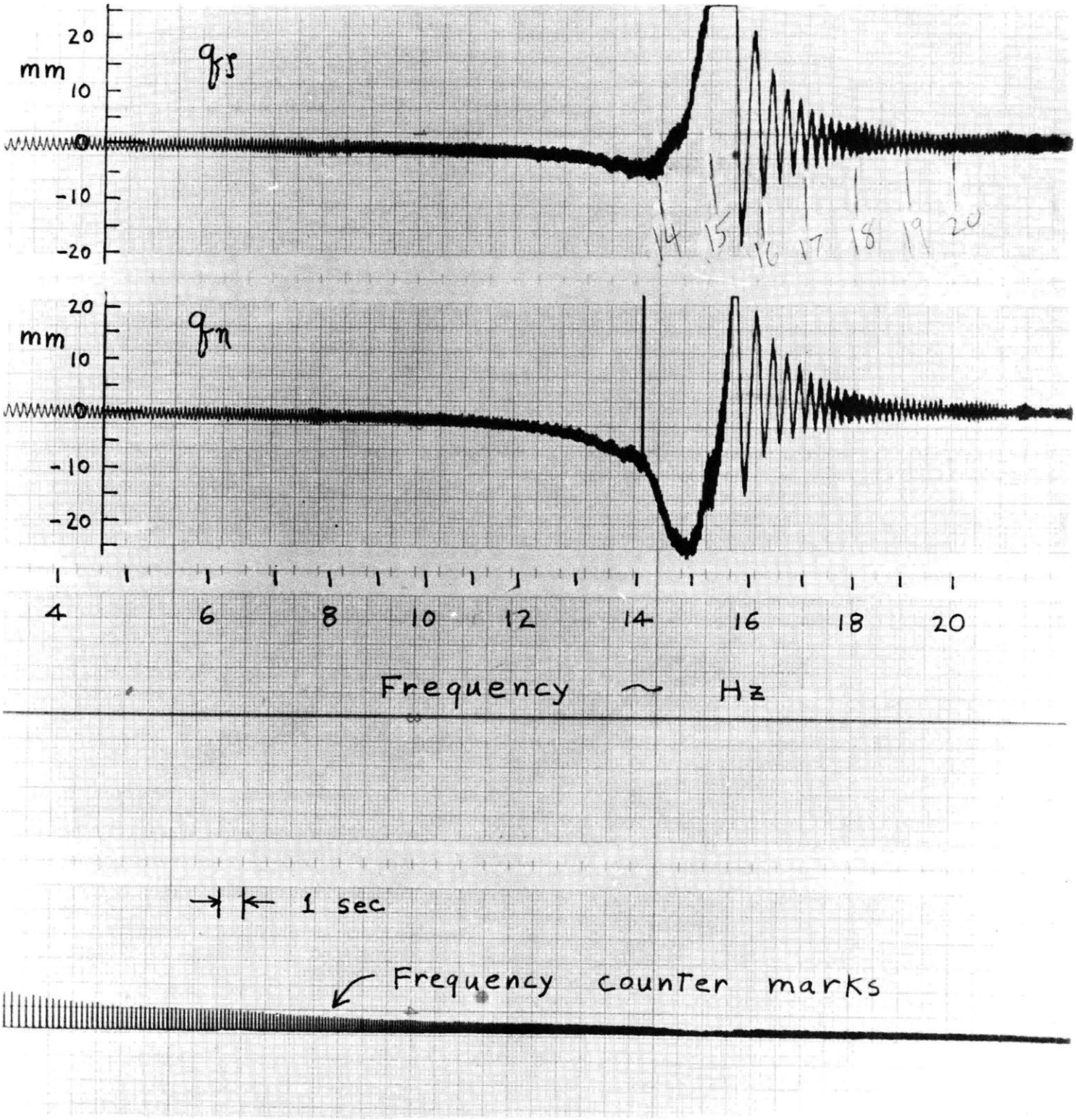

FIG. 8 SHAFT DEFLECTIONS DURING SPEED INCREASE THROUGH CRITICAL SPEED

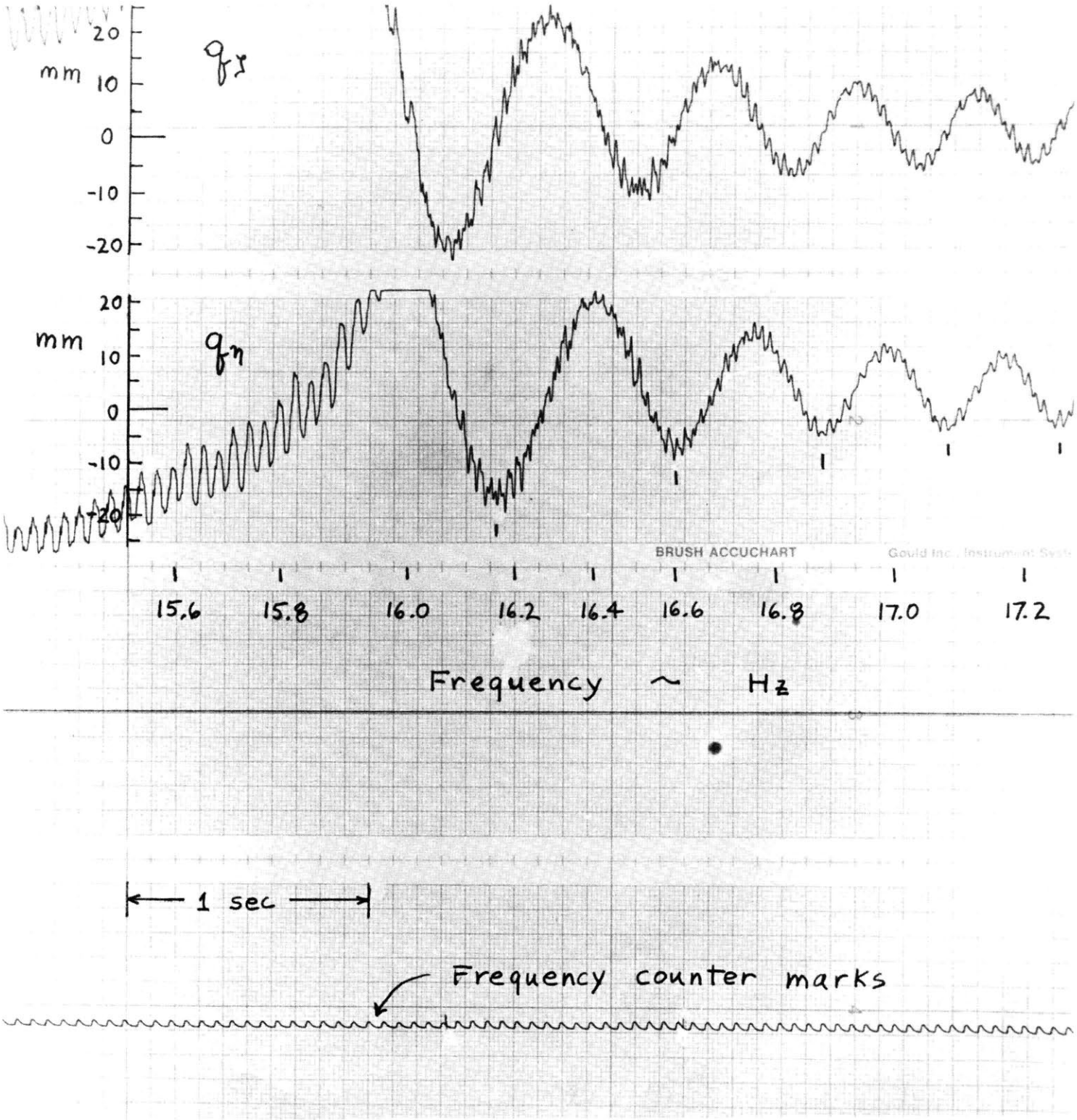

FIG. 9 DETAIL OF SHAFT DEFLECTIONS DURING SPEED INCREASE THROUGH CRITICAL SPEED

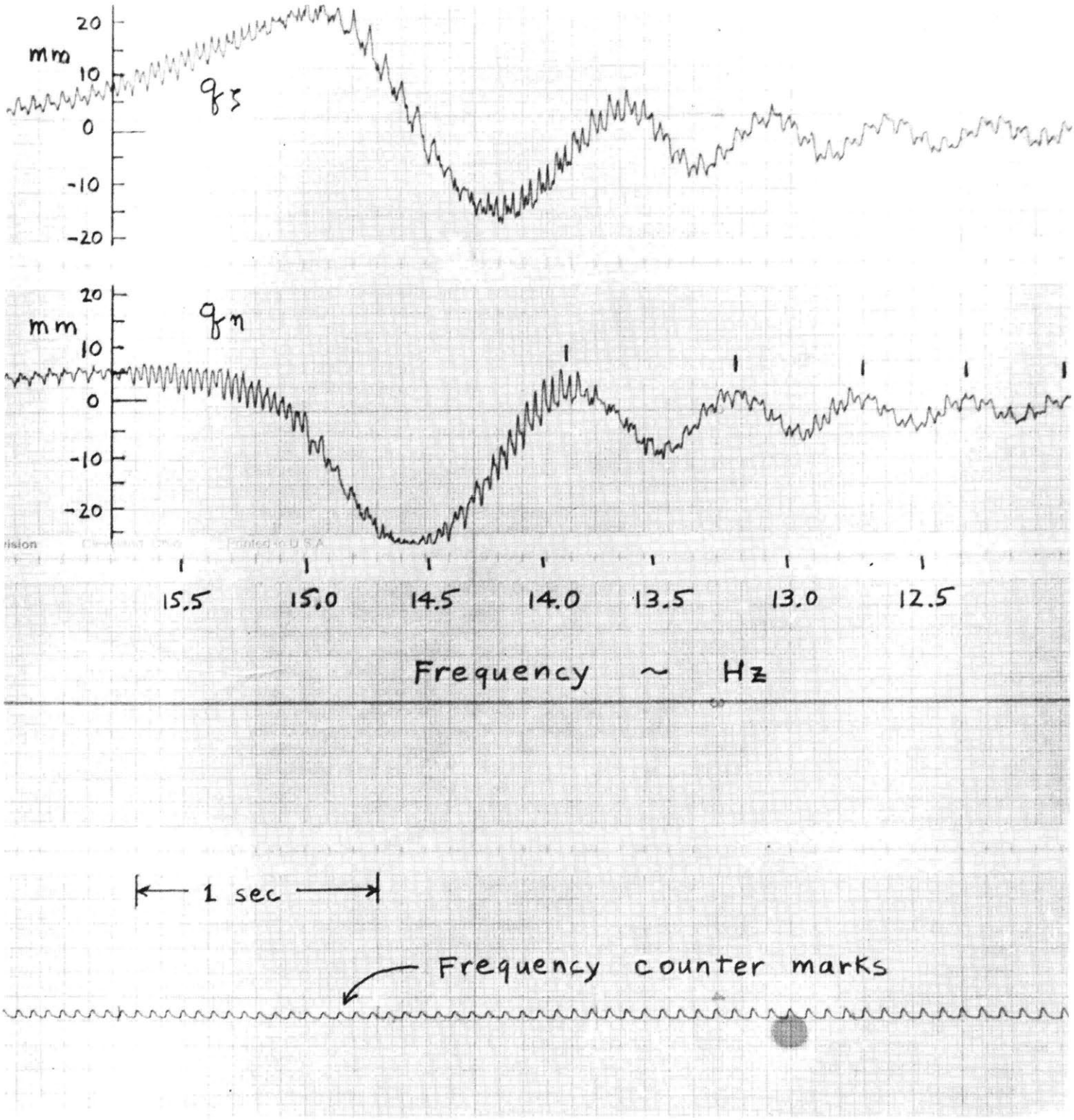

FIG. 10 DETAIL OF SHAFT DEFLECTIONS DURING SPEED DECREASE THROUGH CRITICAL SPEED

FIG. 11 SHAFT ROTATING AT SECOND CRITICAL SPEED

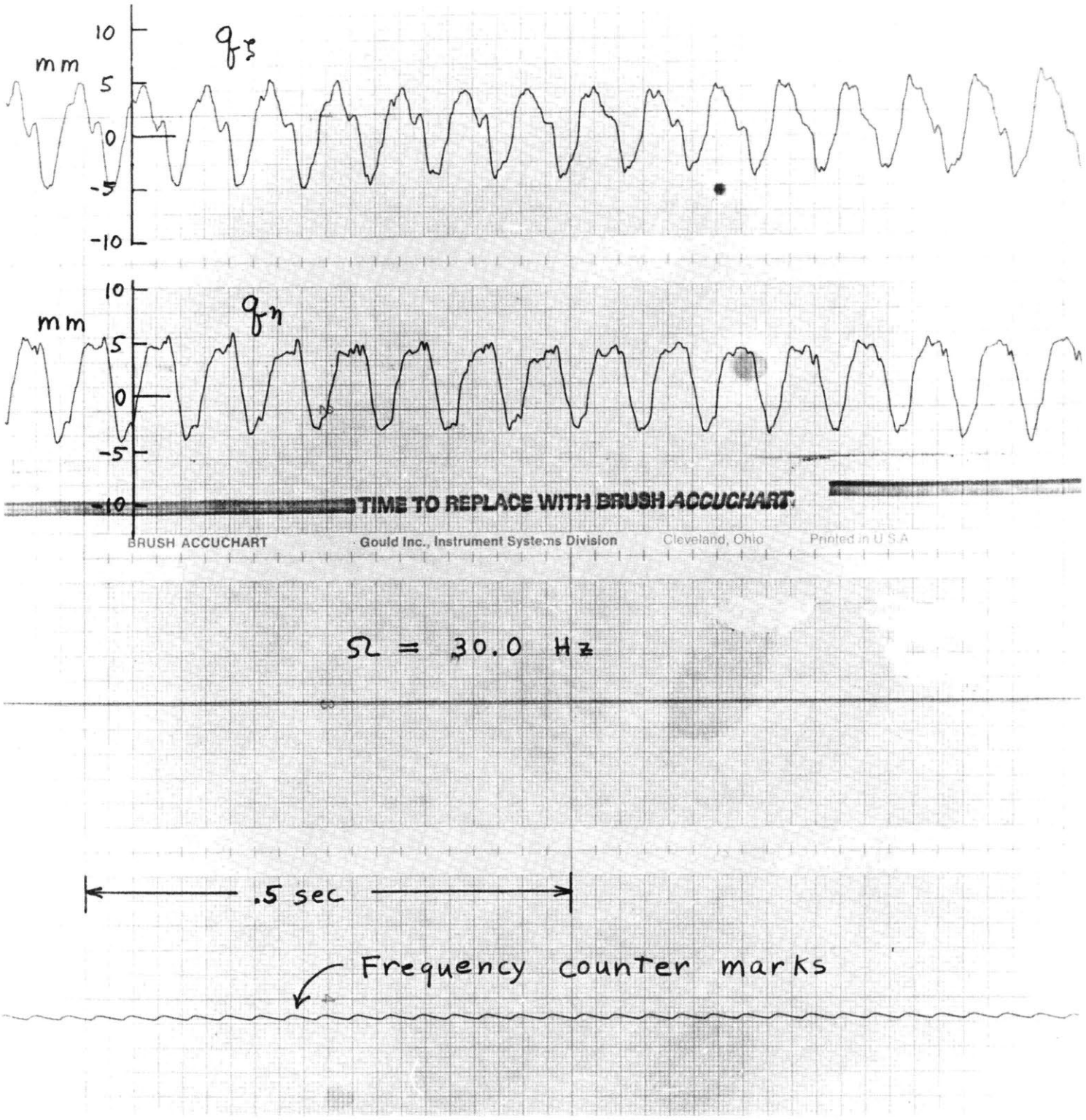

FIG. 12 SUBHARMONIC RESONANCE OF SHAFT